Lunar simulant behaviour in molten fluoride salt for ISRU applications

M. Maes, M. Gibilaro, P. Chamelot, C. Chiron, S. Chevrel, P. Pinet, Laurent Massot, J.J. Favier

Planetary and Space Science 242 (2024) 105854

Contents lists available at ScienceDirect

Planetary and Space Science

journal homepage: www.elsevier.com/locate/pss

Lunar simulant behaviour in molten fluoride salt for ISRU applications

M. Maes [a], M. Gibilaro [a,*], P. Chamelot [a], C. Chiron [a], S. Chevrel [b], P. Pinet [b], L. Massot [a], J.J. Favier [1]

[a] Laboratoire de Génie Chimique, Université de Toulouse, CNRS, INPT, UPS, Toulouse, France
[b] Institut de Recherche en Astrophysique et Planétologie, Université de Toulouse 3 Paul Sabatier, CNRS, CNES, Toulouse, France

ARTICLE INFO

Keywords:
ISRU
Lunar regolith
Molten salt electrolysis
Metal production
Lunar simulant
Joint solubility

ABSTRACT

This study investigated the behaviour of a lunar mare crystalline analog dissolved in molten LiF–NaF at 800 °C for the *in situ* production of metals as a part of In Situ Resource Utilization (ISRU) research. Molten fluorides have the capability to dissolve metallic oxides, and the Hall-Héroult process uses this kind of media to produce Al from Al_2O_3.The first step was to compare the individual solubility of the main oxides composing the mare lunar soil (SiO_2, Al_2O_3, Fe_2O_3, and MgO) with the solubility of the crystalline analog using Inductively Coupled Plasma – Atomic Emission Spectroscopy (ICP-AES). The species concentration added jointly are lower than the concentration of the same species added separately. Nonetheless, this study showed that LiF–NaF can be used to dissolve the analog with a maximum solubility of 3.9 wt% at 800 °C. Cyclic voltammograms were also used to verify the electroactivity of all oxide species in LiF–NaF, wherein all the main oxides are electroactive except SiO_2 and TiO_2. Then electrolyses on different cathodic substrates were performed at different conditions and the obtained cathodic products were analysed with a scanning electron microscope (SEM) coupled with an energy dispersive spectroscopy (EDS). Despite the non-electroactivity of SiO_2 and TiO_2, they were extracted in an alloyed form through Under Potential Deposition (UPD). Metallic deposition of other metals such as aluminium and titanium was achieved on carbon electrode. Finally, a synthetic mixture made of the different oxide species with the same chemical composition as the simulant, was investigated as a viable substitute for lunar mare soil. Its electrochemical behaviour was identical to the crystalline lunar simulant showing that our original process based on oxides dissolution is not influenced by the amorphous/crystalline state of the raw material.

the outputs of LiF–NaF molten process are not critically influenced by the physical state of the lunar regolith.

1. Introduction

Over the last decade, interest in lunar missions has risen drastically. The Artemis program is quite prominent to re-establish human presence on the Moon with Artemis III scheduled in 2025. Other countries such as China, Russia, South Korea, Japan, United Emirates of Arabia, and India are also sending probes and rovers to explore further the surface of the Moon. This increasing interest is not only because of the future context of human extraterrestrial settlement but also due to the recent discovery of water at the south pole of the Moon. The main space agencies believe that extended missions on the Moon could serve as a training ground for the future missions to Mars. To settle down in space, the utilization of local resources is mandatory. The primary objective is to turn these lunar resources into useful life elements such as oxygen and metals. The top layer of the Moon consists in a regolith which results from multiple impacts on the original rocks emplaced on the surface by different geological processes. It comprises metallic oxides (40–45 % wt oxygen), as shown in Fig. 1. This data had been originally summarized by Schlüter and Cowley (2020) and was recently updated with data from Chang'e−5 samples.

The main component of lunar soil is SiO_2, with a concentration ranging from 40.6 wt% to 48.1 wt%. Other oxides such as Al_2O_3 and FeO display larger ranges of concentrations, 6.3–28.0 wt% and 4.7–24.5 wt% respectively, depending on whether they are found in highlands (made of anorthositic materials) or mare soils (basaltic materials). Furthermore, up to 8.4 wt % of TiO_2 in the form of ilmenite ($FeTiO_3$) is found in mare basalts (McKay et al., 1991). Thus, the lunar soils offers a variety of metals which could be extracted for manufacturing and construction purposes. Moreover, oxygen could be recovered during the extraction process and used as propellant and life support systems. After the Apollo

* Corresponding author.
E-mail address: mathieu.gibilaro@univ-tlse3.fr (M. Gibilaro).
[1] Deceased.

https://doi.org/10.1016/j.pss.2024.105854
Received 3 November 2023; Received in revised form 15 January 2024; Accepted 6 February 2024
Available online 4 March 2024

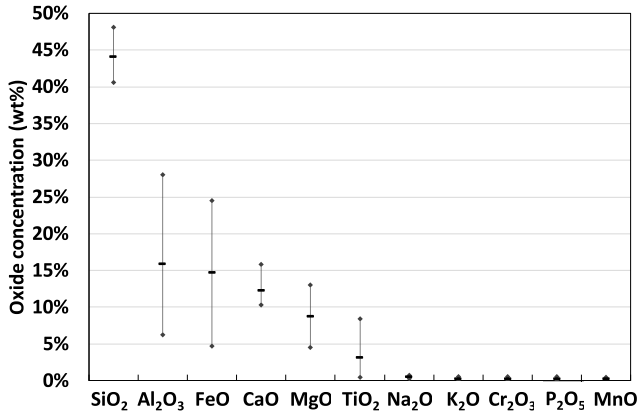

Fig. 1. Average (−), minimum and maximum abundance of major oxides in lunar landing sites in wt% (data from (McKay et al., 1991) for Apollo and Luna samples, (Ling et al., 2015) for Chang'e−3 samples and (Che et al., 2021; Li et al., 2022; Chen et al., 2023) for Chang'e−5 samples.

Era, a wide range of different processes were studied including hydrogen reduction, carbothermal reduction, fluorination, vacuum pyrolysis, molten regolith electrolysis and molten salt electrolysis to extract metals and oxygen from lunar regolith (Schwandt et al., 2012; Anand et al., 2012; Schlüter and Cowley, 2020; Shaw et al., 2022; Zhang et al., 2023). These processes can be mainly distinguished by the lunar regolith state (solid, liquid or vapour) which depends on the operating conditions used during the process. Since no lunar samples are available for ISRU investigations which often require significant amounts of material, lunar soil simulants were developed to address the engineering studies. Some of the existing lunar simulants derived from terrestrial geological materials were reviewed by Taylor and Liu in 2010 (Taylor and Liu, 2010). The production of lunar regolith simulants, their history, their use and misuse are described in 2016 by Taylor et al. (2016). The environmental conditions existing on the Moon make it challenging to replicate a perfect simulant, but it is possible to produce lunar analogs from terrestrial materials having for instance similar bulk chemistry than lunar rocks and soils. One example is the LMS-1 Lunar mare simulant which has an accurate texture and bulk chemistry (Exolith Lab, 2023), and was used in several ISRU studies (Isachenkov et al., 2022a, 2022b; Meurisse et al., 2022; Sargeant et al., 2022; Schein et al., 2022).

Hydrogen or carbothermal reductions use the interaction of a specific gas with lunar regolith materials to extract oxygen. In this case, the lunar regolith is put in contact with a flow of hydrogen at 700–1100 °C or methane at 1100–1650 °C. The oxygen is extracted in the form of water vapour (Eq. (1)) and is oxidised in pure oxygen through water electrolysis (Eq. (2)).

$$FeTiO_{3(s)} + H_{2(g)} \rightarrow Fe^0 + TiO_2 + H_2O_{(g)} \quad (1)$$

$$2\,H_2O_{(l)} \rightarrow 2\,H_{2(g)} + O_{2(g)} \quad (2)$$

Based on well-established industry applications, a lot of research was done in hydrogen reduction (Williams, 1985; Gibson et al., 1994; Allen et al., 1996; Hegde et al., 2009; Lu et al., 2010; Sanders Gerald B. and Larson William E., 2013; Denk et al., 2017; Kumai et al., 2021; Sargeant et al., 2021) and carbothermal reduction ((Cutler and Krag, 1985; Rosenberg et al., 1992; Sen et al., 2005; Lu and Reddy, 2008; Kobayashi et al., 2010; Peng et al., 2022; Troisi et al., 2022). The drawbacks of these processes are the need of ilmenite ($FeTiO_3$) in the feedstock, use of consumable reagents, multiple steps to produce O_2 gas and the presence of an artificial atmosphere. In the case of carbothermal reduction, utilizing molten regolith enables the reduction of large amounts of metallic oxides, yet it complicates the process.

Lunar regolith can also be vaporised under vacuum conditions at temperatures above 1000 °C in order to retrieve oxygen and metals. High working temperatures can be achieved by different means such as solar concentrator technologies (Gordon et al., 2011; Palos et al., 2020) and microwave heating (Lim et al., 2023). This process is called vacuum pyrolysis or vapour phase reduction. After vaporising the lunar regolith, the oxides are decomposed into metals and oxygen: the metals are condensed whereas the oxygen remains gaseous (Steurer and Nerad, 1983; Senior, 1992; Cardiff et al., 2007; Schubert, 2007; Kate et al., 2010; Shaw et al., 2021). The main difficulty in this process is to properly separate the metals, metals oxides, and oxygen from the mainstream.

The final option, as discussed in this paper, is to reduce regolith using electrolytic processes. Lunar regolith has a high fusion temperature and is fully melted above 1600 °C. During the polarisation, the oxide anions (O^{2-}) are transported through the molten regolith and are oxidised into pure oxygen gas (Eq. (3)) whereas the metallic cations (M^{n+}) are reduced as liquid or solid metal on the cathode (Eq. (4)).

$$2\,O^{2-} \rightarrow O_2 + 4\,e^- \quad (3)$$

$$M^{n+} + n\,e^- \rightarrow M \quad (4)$$

Because of the high operating temperatures, only a few noble metals such as iridium (Kesterke, 1971; Sibille et al., 2009), rhodium and platinum (Gmitter, 2008), 50-50 iridium/tungsten (Vai et al., 2010) or ceramic materials can be used as electrodes. The presence of iron in the feedstock also limits the current efficiency to 30–60% due to the reversible reaction of Fe^{3+}/Fe^{2+} (Sibille et al., 2009). However, the main advantage of the process is its multi-component lunar feedstock, but its high working temperature induces a highly corrosive environment. Kim et al. (2011) showed that the corrosion rate of iridium anode increased with the basicity of the electrolyte (high CaO rate). Therefore, these conditions make it difficult to find an inert anode, which remains the main engineering problem of the molten regolith electrolysis.

A promising alternative is the use of molten salts as electrolyte and to apply a direct or indirect electro-deoxidation of the solid regolith material. One way is through the Fray Farthing Chen (FFC) Cambridge process which involves the direct electrochemical reduction of solid-state metallic oxide into metal and oxygen (Eq. (5)) in molten $CaCl_2$ at around 900 °C (Fray, 1999; Chen et al., 2000; Schwandt et al., 2010).

$$M\,O_y + 2y\,e^- \rightarrow M + y\,O^{2-} \quad (5)$$

The oxide anions (O^{2-}) react at the conventionally used graphite anode to form CO and/or CO_2 (Eqs. (6) and (7)).

$$O^{2-} + C \rightarrow CO + 2e^- \quad (6)$$

$$2\,O^{2-} + C \rightarrow CO_2 + 4e^- \quad (7)$$

Lomax et al. (2020) used the Johnson Space Center lunar soil simulant (JSC-2A) in $CaCl_2$ at 950 °C. In their study the graphite anode was replaced by an oxygen evolving anode (SnO_2). Electrolysis of 52 h was conducted with a fixed current of 4 A on 30g of lunar simulant. The total oxygen detected by mass spectrometry was about 34% of the oxygen present in the starting material. However, the SnO_2 anode encountered both mechanical and chemical issues. The composition of the reduced solid products was analysed by oxygen analysis and SEM/EDX. A total oxygen extraction of 96% was observed and different alloys/phases were obtained.

- Al/Fe alloy (3:1 Al to Fe ratio) with inclusions of silicon up to 10%,
- Fe/Si alloy containing Ti and/or Al in significant amount mostly located in Al/Fe,
- Ca/Si/Al phase with the inclusion of Mg.

Meurisse et al. (2022) studied a 24 h electrolysis at 3.2 V of lunar mare simulant LMS-1 (Exolith Lab, 2023) in different $CaCl_2$-based

eutectic salts between 660 °C and 950 °C: $CaCl_2$; $CaCl_2$–KCl; $CaCl_2$–NaCl and $CaCl_2$–LiCl. A temperature-dependent oxygen extraction efficiency was observed with an optimal working temperature of 680 °C in $CaCl_2$–NaCl. A current efficiency above 60% was obtained with an oxygen removal higher than 40%. Moreover, experiments with all eutectics at 950 °C showed that the efficiency of the reaction is also related to the $CaCl_2$ content and the associated CaO solubility and different metallic phases (Si/Ca and Si/Ti/Fe) were observed when LiCl was added.

Recently, Shi et al. (2022) worked with solid Chang'e−5 lunar regolith simulant in $CaCl_2$ at 850 °C. An electrolysis at 3 V for 12 h produced metallic products with the following mass fractions: 43.43 wt % Fe, 31.68 wt% Si, 11.45 wt% Ti, 8.72 wt% Al, 3.57 wt% Cr and less than 1 wt % Ca, Mg and Mn. A current efficiency of 43.4% was observed with an energy consumption of 12.3 kWh/kg O. In this study, the usual graphite anode was used but a secondary cell was required to transform the produced CO/CO_2 gas into O_2, containing a Li_2CO_3–Na_2CO_3–K_2CO_3 (molar ratio 43.5:31.5:25.0) molten electrolyte at 650 °C. A Ni alloy and Pt/Ti anodes were used as working electrodes. An electrolysis of 2 A for 5h on Ni alloy anode produced a rising flow of oxygen and eventually became stable at 20.4 vol% after 3.7h. Similar observations were made for the Pt/Ti anode.

Ellery et al. (2022) proposed several chemical pre-processes to enhance the products obtained by FFC Cambridge process. An artificial weathering approach using HCl is discussed, through which the electrolyte $CaCl_2$ is produced as a by-product. Different metal 3D printing techniques are considered to manufacture components and systems of robotic machines of production.

Another direction of research worth to be explored is the use of a fluoride salt known to dissolve metallic oxides and amorphous SiO_2 (glass), such as the Hall-Héroult process where Al is produced from aluminium oxide in molten Na_3AlF_6 at 970 °C: aluminium cations are reduced at the cathode and oxygen anions react with the carbon anode to form CO and CO_2. Xie et al. (2017) worked with Minnesota Lunar Simulant MLS-1 (5.27 mass%) in cryolite melts at 960 °C on liquid Al cathode and a ferronickel ($Fe_{0.58}$-$Ni_{0.42}$) inert anode. After a 4h electrolysis at 0.9 A cm^{-2}, gas chromatography confirmed the production of pure oxygen with an average anodic current efficiency of 78.28%. The cathodic products were analysed by X-ray diffraction (XRD) and X-ray fluorescence (XRF) analyses, wherein the main metallic phase obtained was aluminium with traces of other elements composing lunar regolith. A cathodic current efficiency of 55.43% was calculated. The loss of current efficiency was explained by the dissolution of deposited Al into the electrolyte, the formation of alloys with the other present metals, the formation of a yellow green layer (Al_4C_3) at the bottom of the crucible and the presence of multivalence titanium ions and silicon ions (Xie et al., 2017). Another study in cryolite melt done by Liu et al. (2017) was conducted with NEU-1 simulant (5 wt%) in NaF–AlF_3 at 960 °C. A similar ferronickel inert anode was used for oxygen production and a graphite rod as cathode. Galvanostatic electrolysis at 0.9 A cm^{-2} of 8h resulted in obtaining a cathode product with 2 intermetallic phases: Al–Si and Al–Si–Fe.

Studies in cryolite melts have demonstrated that oxides mixtures such as lunar simulants can be partially dissolved in fluoride-based mixtures at high temperatures. In this paper, further investigation is implemented with a fluoride-based mixture made of LiF–NaF (61-39 mol %) which melts at 652 °C. The working temperature of 800 °C, typically used in this medium, was chosen as a first process demonstration.

Different types of surrogate were investigated at 800 °C.

- a Natural lunar mare simulant called *Basalte Pic d'Ysson* referred as BPY-N.
- the oxides composing BPY-N individually studied.
- and a mixture of these individual oxides to reproduce the chemical composition of BPY-N called BPY-Synthetic-Oxide-Powder (BPY–SOP).

The solubility of the individual oxides and the lunar simulant was measured through Inductively Coupled Plasma – Atomic Emission Spectroscopy (ICP-AES). The different surrogates were investigated through electrochemical means such as cyclic voltammetry and electrolysis. Their electroactivity was verified by cyclic voltammetry on a molybdenum cathode. This study is focused on the cathodic part; the anodic part is beyond the scope of this paper and will be addressed separately in a companion paper. Several electrode materials were studied to show the possible extraction of metals from the lunar soil. The composition of the deposited metal depends on the nature of the substrate. Molybdenum, iron and carbon electrodes were tested to investigate which metal/alloy was obtained during the deposition.

A synthetic oxide powder mixture was investigated as a viable substitute for lunar mare soil. The electroactivity and metal extraction of natural lunar simulant BPY-N were compared with the results produced from a synthetic lunar simulant (BPY–SOP) made of a mixture of oxides similar to the composition of BPY-N. These different solutes have the same chemical composition but different crystalline structures. In order to assess to what extent the physical state could possibly affect the electrochemical behaviour along the process, BPY-N and BPY-SOP were thus compared to document the influence of the microstructure of the solute in the molten salt process.

2. Materials and methods

2.1. The cell

The setup used for the electrochemical experiments is presented in Fig. 2 which comprises the cell, molten salts, samples (BPY–N, individual metallic oxides, BPY-SOP), and electrodes.

The electrochemical experiments were carried out under argon atmosphere (99.995 vol%, Linde) in a vitreous carbon crucible placed inside a circular vessel made of refractory steel and closed by a steel lid in which a flow of cooled water circulates. A graphite liner protects the inside walls against fluoride vapours. The cell was heated using a programmable furnace and the temperatures were monitored using a chromel-alumel thermocouple. An airlock was used to introduce samples into the molten salts avoiding air entrance in the reactor.

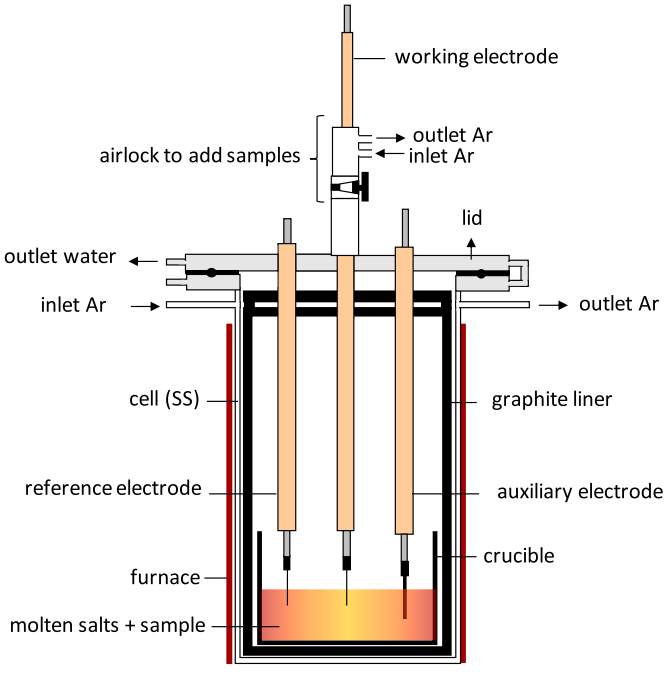

Fig. 2. Setup of the electrochemical experiments.

2.2. The salts

200 g of LiF–NaF (99.99%, Fox Chemical GmbH), at eutectic composition (61-39 mol%), was initially dehydrated by heating under vacuum (8×10^{-2} atm) from ambient temperature up to its melting point for one week.

2.3. The natural lunar simulant: Basalte Pic d'Ysson (BPY–N)

A natural close analog to the Lunar Mare Simulant LMS-1, called "*Basalte Pic d'Ysson*" (Souchon et al., 2011; Granier et al., 2022) named BPY-N and provided by the Institute of Research in Astrophysics and Planetology (IRAP) of Toulouse, was used in this study. The composition of the LMS-1 and BPY-N lunar simulants are given in Table 1 and are compared with an Apollo 11 bulk mare soil sample (Papike et al., 1982).

It is important to emphasise that the chemical species presented in Table 1 are not present in the simulant in their pure oxide form: instead, they exist as mineral and amorphous phases. Furthermore, BPY-N is composed of ferric ions which are normally not present on the Moon due to the highly reducing environment. However, recent studies (Gu et al., 2023) have suggested the existence of these species within amorphous silicates in Chang'e−5 samples. Anyhow, the influence of the Fe valence was investigated in this publication.

The bulk chemistry of the lunar simulants made from terrestrial materials is close to the chemistry of samples brought back from the Moon. They are therefore commonly used as analogs (study material) for ISRU purposes.

BPY-N is a fresh basalt recovered from a lava flow of *Pic d'Ysson* (Massif Central, France). It contains phenocrysts of olivine, pyroxene, and plagioclase. For the purpose of our studies, it was mechanically ground and sieved. The particle size distribution is as follows: Dv (10) = 6 μm; Dv (50) = 131 μm; Dv (90) = 432 μm.

2.4. Individual metallic oxides

The oxides composing lunar soil were individually studied in their powder form: SiO_2, MgO (Neyco 99.95%), Fe_2O_3 (Alfa Aesar 99.9% metals basis), Al_2O_3 (Alfa Aesar 99% metals basis), $FeTiO_3$ (Alfa Aesar 99.8% metals basis) and TiO_2 (Sigma-Aldrich 99.98% metals basis).

2.5. BPY-Synthetic-Oxide-Powder (BPY–SOP)

A BPY-Synthetic-Oxide-Powder (BPY–SOP) mimicking the BPY-N composition (see Table 1) has been prepared by mixing size-controlled powder of the main metallic oxides mentioned above (see 2.4 Individual metallic oxides) and completed with the following metallic oxides: CaO (Alfa Aesar 99.95 % metals basis) and Na_2O. The composition of BPY-SOP is presented and compared to BPY-N in Table 2.

Table 1
Comparison of bulk chemistry between a sample of Apollo 11 in mare region, LMS-1 and BPY-N simulants.

Oxide	Bulk Chemistry (wt.%)		
	LMS-1	BPY-N	Apollo 11 sample 10084, 1591
SiO_2	46.9	42.8	41.3
Al_2O_3	12.4	11.5	13.7
FeO	8.6	/	15.8
Fe_2O_3	/	12.9	/
MgO	16.8	15.3	8
CaO	7	9.6	12.5
TiO_2	3.6	2.1	7.5
Na_2O	1.7	2.7	0.4
K_2O	0.7	1.2	0.1
P_2O_5	0.2	0.6	/
MnO	0.2	0.3	0.2
Cr_2O_5	/	/	0.3

Table 2
Comparison of bulk chemistry between BPY-N and BPY-SOP

Oxide	Bulk Chemistry (wt.%)	
	BPY-N	BPY-SOP
SiO_2	42.8	45.9
Al_2O_3	11.5	11.5
Fe_2O_3	12.9	12.9
MgO	15.3	15.3
CaO	9.6	9.6
TiO_2	2.1	2.1
Na_2O	2.7	2.7
K_2O	1.2	/
P_2O_5	0.6	/
MnO	0.3	/

The size controlled powders were mixed for 1 h in a powder mixer at 20 rpm (Robin materiel de Laboratoire). Accordingly, BPY-SOP has a similar bulk chemistry but does not have the same texture and crystallographic properties.

2.6. Electrodes

Molybdenum, iron wires (Goodfellow 99.99%, 1 mm diameter), and carbon rod (Goodfellow 99.99%, 3 mm diameter) were used as working electrodes. The auxiliary electrode was a vitreous carbon rod (3 mm diameter) with a large surface area (5 cm^2). The quasi-reference electrode was a platinum wire (Alfa Aesar 99.95%, 1 mm diameter).

2.7. Analytical techniques

2.7.1. Electrochemical analysis

Electrochemical studies and electrolyses were performed with an Autolab PGSTAT 302N potentiostat/galvanostat controlled with Nova 2.1.5 software. All the potentials were referred to the equilibrium potential of NaF/Na system on the cyclic voltammograms plotted using an inert molybdenum working electrode. Cyclic voltammetry is commonly used in electrochemistry to study redox reactions and electrochemical behaviour of chemical compounds. A potential is applied, and a corresponding current is measured resulting in peaks which are characteristic of a reaction occurring at the electrode. Cyclic voltammetry was used for the investigation of the reduction pathway of the major oxides composing lunar soil and lunar simulant. Metal deposition was achieved using electrolysis, a technique that involves applying an electric potential (potentiostatic electrolysis) or current (galvanostatic electrolysis) for a specific duration.

2.7.2. ICP-AES analysis

The metal oxide solubility in the fluoride-based solvent was measured through Inductively Coupled Plasma – Atomic Emission Spectroscopy (ICP-AES, Horiba Jobin Yvon Ultima 2) by sampling 100 mg of salt. A total liquid solution is required to perform ICP-AES analysis; therefore, a dissolution method was created using a mixture of strong acids (HF, HCl, HNO_3, and H_2SO_4). After the analysis, the element concentration was determined.

2.7.3. Deposits observations

The deposit at the electrodes was monitored and characterized by a Phenom XL scanning electron microscope (SEM) coupled with an energy dispersive spectroscopy (EDS).

3. Results and discussion

3.1. Lunar soil oxides solubilities in molten LiF–NaF at 800 °C

The solubility of the individual oxides and BPY-N was measured through ICP-AES measurements. The goal is to determine the dissolution

yield of the different individual oxides and lunar simulant in the LiF–NaF solvent. The working temperature of 800 °C, typically used in this medium, was chosen as a first demonstration to study this process.

3.1.1. Solubility of the individual oxides

The individual oxides (SiO_2, Al_2O_3, Fe_2O_3, TiO_2, MgO and CaO) that compose the lunar soil were put separately in molten LiF–NaF at 800 °C.

The concentration of the individual oxides was measured following this procedure.

- Mixtures were prepared by adding 20 wt% of each individual oxide into LiF–NaF.
- The mixtures were heated to 800 °C for 2 days.
- Samples of 100 mg were taken directly from the molten bath and analysed through ICP-AES analysis after acidic dissolution.

ICP-AES is based on exciting the metal atoms using an inductively coupled plasma and analysing the emission wavelength of the electromagnetic radiation, which is characteristic of that particular metal atom. Each metallic element has one or more specific wavelengths, some of these can be affected by the presence of the solvent. To select the working wavelength for each element, the matrix effect must be evaluated first. The specific wavelengths selected for each element are summarized in Table 3.

These wavelengths were used to measure the elemental concentration of the metal oxides. After taking into account the matrix effects, the individual solubility was established for each individual oxide. The ICP-AES measurement gives the concentration of the metallic element in ppm. From this element concentration, the equivalent oxide concentration was established by using the metallic mass ratio for each oxide: for instance, Si represents 47 wt% of SiO_2. After knowing the amount of SiO_2 dissolved, dividing it by the mass of the solution, the solubility of each oxide in LiF–NaF at 800 °C is determined. The individual solubility for each oxide is presented in Table 4.

The oxide with the lowest solubility is Al_2O_3 with only 2.8%, whereas SiO_2 has the highest with 17.4%. This finding is particularly significant considering that the lunar soil contains a high concentration of SiO_2.The second most soluble oxide in LiF–NaF at 800 °C is Fe_2O_3 with 15.7% followed by MgO with 12.4%, and TiO_2 with 4.8%. From these results, we demonstrate that all the major oxides composing mare lunar soil are thus partially dissolved in LiF–NaF at 800 °C.

3.1.2. Solubility of lunar simulant BPY-N

ICP-AES measurements were performed following the same procedure as described in 3.1.1 on different additions of lunar simulant BPY-N in LiF–NaF at 800 °C. The main oxides of BPY-N (SiO_2, Fe_2O_3, MgO, Al_2O_3, TiO_2 and CaO) were investigated. However, TiO_2 concentration values are not presented as a very low signal was recorded: the obtained values were not reliable. Results are shown in Fig. 3, depicting the variation of the oxide concentration versus BPY-N mass fraction. These experimental concentrations are compared to their theoretical values, which correspond to the fully dissolved oxide and are represented as a line. The left Y-axis is for the wt% concentration of SiO_2 and the right Y-axis corresponds to the other oxides concentration (wt%). The vertical line at 3.9 wt% indicates the maximum solubility of BPY-N reached.

Table 3
Summary of the wavelengths for the major elements composing lunar simulant.

Element	Wavelengths (nm)
Si	288.2
Mg	279.1
Fe	300.1
Al	394.4
Ca	317.9
Ti	338.4

Table 4
Summary of the individual solubility of the major oxides composing lunar soil in LiF–NaF at 800 °C.

Oxide	Individual solubility wt% (g oxide/g solution)
SiO_2	17.4% ± 0.9
Fe_2O_3	15.7% ± 0.6
MgO	12.4% ± 0.4
TiO_2	4.8% ± 0.4
Al_2O_3	2.8% ± 0.4

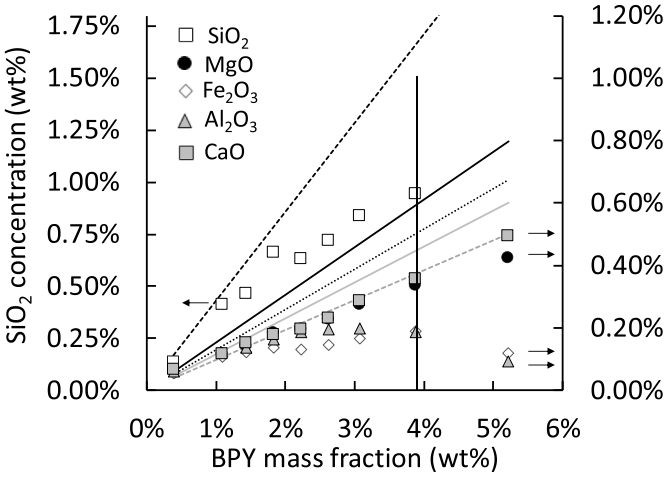

Fig. 3. Illustration of the joint solubility effect by comparing the evolution of the oxide concentration to their theoretical concentration for different additions of BPY-N (X-axis) in LiF–NaF at 800 °C. The lines correspond to the theoretical concentration of the oxide: SiO_2 (– – –•); MgO (——); Fe_2O_3 (·····); Al_2O_3 (——) and CaO (- - - -). The symbols correspond to the experimental concentrations measured through ICP-AES means. The left Y-axis is the wt% concentration of SiO_2 and the right Y-axis corresponds to the wt% concentration of the other oxides. Arrows indicate the Y axis corresponding to the oxide concentration. A vertical line at 3.9 wt% indicates the maximum solubility.

The concentration of CaO increases linearly, in agreement with the added content of BPY-N. The concentration of all other oxides does not vary linearly, indicating that the dissolution of these species is not complete. In the case of Al_2O_3 and Fe_2O_3, it can be observed that their concentrations decrease beyond 3.9 % BPY-N mass fraction. The more BPY-N is added to the LiF–NaF system, the more the equilibrium concentration of each oxide (except CaO) deviates from the theoretical concentration. For instance, for 3.9 wt%, a relative deviation of 43.2%, 43.5%, 58.2% and 62.4% of the concentration is observed for SiO_2, MgO, Al_2O_3 and Fe_2O_3, respectively. When different oxides are mixed, the individual solubility of each metal is significantly lowered because of the joint solubility effect. Lizin et al. already observed this phenomenon with PuF_3 and UF_4 in a LiF-NaF-KF solvent where the individual solubility of these compounds was reduced by 2–5 times when mixed together between 550 and 800 °C (Lizin et al., 2015). In molten fluoride melts, different complexes are made among the free fluoride ions, oxide anions and the metallic cations to form anionic species (Bessada et al., 2020; Feng et al., 2021; Kuznetsova et al., 2009; Mysen and Virgo, 1985). The formation of these complexes leads to a competition among the different cations for the available fluoride ions causing a decrease in individual solubility. The highest joint solubility effect was observed at 3.9 wt% LiF-NaF-BPY-N, wherein the dissolution yield was determined by dividing the calculated mass of equivalent metallic oxides by the total mass of BPY-N added (Eq. (8))

$$Dissolution\ yield = \frac{\sum_i (calculated\ mass\ of\ equivalent\ metallic\ oxides)}{Total\ mass\ of\ BPY-N} \quad (8)$$

The dissolution yield is equal to 63 wt%, which opens an interesting possibility for metal production by this kind of electrolytic process. Indeed, the solubility observed of BPY-N in LiF–NaF indicates that metals can be efficiently produced in a electrochemical way.

3.2. Electrochemical analysis

Metal deposition through electrochemical methods is possible only when the metallic element is both soluble in the medium and electroactive. However, when dealing with mixtures of various metallic oxides, such as BPY-N, the electrochemical analysis produces a complex signal that makes it challenging to discern the reactions taking place. In order to understand this complex signal, cyclic voltammograms were used on separate metallic oxide solutes in LiF–NaF at 800 °C.

- MgO, TiO_2, Fe_2O_3, $FeTiO_3$, SiO_2 and Al_2O_3 were individually analysed in the medium to observe their solubility and electroactivity.
- Mixtures of SiO_2/Al_2O_3, SiO_2/Fe_2O_3 and $SiO_2/Al_2O_3/Fe_2O_3$ were used to observe the influence on the metallic elements solubility and behaviour when they are mixed together in the same medium.
- Natural lunar simulant BPY-N was investigated by electrochemistry and its behaviour was compared with a synthetic lunar simulant BPY-SOP.

3.2.1. Individual oxides

The electroactivity of the individual oxides was verified with cyclic voltammetry. The following cyclic voltammograms were performed on a Mo electrode and carried out at 800 °C in LiF–NaF. The anodic and cathodic limits correspond to the oxidation of the working electrode material (Mo) and the solvent reduction respectively. All the potentials were referred to the equilibrium potential of the NaF/Na system.

3.2.1.1. MgO in LiF–NaF at 800 °C. Fig. 4 shows the typical cyclic voltammogram plotted on the Mo electrode at 800 °C and 3.75 wt% MgO in LiF–NaF at 100 mV s^{-1}.

An electrochemical signal is observed for MgO, confirming its solubility in LiF–NaF at 800 °C in agreement with the ICP-AES measurements seen in 3.1. A complex system made of several different redox systems is observed between 0.02 and 1.40 V vs NaF/Na. However, it can be noted that the reduction of MgO species occurs at lower potential than 1.4 V vs NaF/Na. Thus, the complexity of the signal makes it difficult to identify the MgO reduction mechanisms.

3.2.1.2. TiO_2, Fe_2O_3 and $FeTiO_3$ in LiF–NaF at 800 °C. Ti oxides are present in the lunar soil at one oxidation state (IV) and was thus studied as TiO_2 in this publication. The multiple valences (II or III) of iron were taken into account in the electrochemical investigation: Fe (II) was studied as $FeTiO_3$ and Fe (III) as Fe_2O_3. Fig. 5 presents a cyclic voltammogram plotted on Mo electrode at 100 mV.s^{-1} of LiF–NaF–TiO_2 (1.5 wt%), LiF–NaF–Fe_2O_3 (2.25 wt%) and LiF–NaF– $FeTiO_3$ (1.75 wt%) systems at 800 °C.

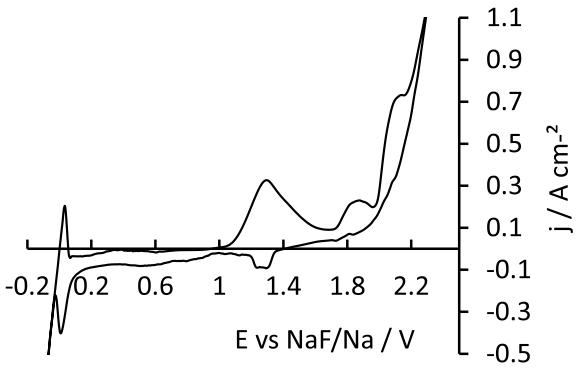

Fig. 4. Cyclic voltammogram of LiF–NaF–MgO (3.75 wt%) system on Mo electrode at 100 mV s^{-1} and T = 800 °C.

No electrochemical activity was observed for TiO_2 while its solubility in LiF–NaF at 800 °C was confirmed by ICP-AES measurements: TiO_2 is thus not electroactive in LiF–NaF. The same electrochemical signal is observed for $FeTiO_3$ and Fe_2O_3, although their different oxidation states: an oxidation peak and cathodic peak are observed around 1.62 and 1.5 V vs NaF/Na respectively. This indicates the reduction of the same species at 1.5 V vs NaF/Na. The cathodic peak has an asymmetric shape (1) indicating the formation of an insoluble compound during the cathodic scan and the reoxidation peak has a stripping shape (2) which is characteristic of a solid phase redissolution. Based on these comments, only Fe(II) is present in the solvent. the spontaneous reduction of Fe(III) to Fe (II) takes place upon the dissolution of Fe_2O_3 in LiF–NaF at 800°.

3.2.1.3. SiO_2 and Al_2O_3 in LiF–NaF at 800 °C. A cyclic voltammogram plotted on Mo at 100 mV s^{-1} of LiF–NaF with 1.65 wt% SiO_2, 3.75 wt% Al_2O_3 and 3.75% Al_2O_3 + 1.65 wt% SiO_2 can be found in Fig. 6.

Cathodic signals are observed for LiF–NaF–Al_2O_3 at 0.3 and 0.16 V vs NaF/Na with corresponding oxidation peaks at 0.35 and 0.49 V vs NaF/Na confirming the solubility of Al_2O_3 in LiF–NaF at 800 °C. The reoxidation peak (1) at 0.49 v vs NaF/Na exhibits a stripping shape typical of a solid phase redissolution, thereby confirming the reduction of Al ions. No reaction takes place for SiO_2, whereas it was confirmed by ICP-AES measurements that SiO_2 is soluble in LiF–NaF at 800 °C: as for TiO_2, SiO_2 is not electroactive in this solvent. For a bath containing both Al_2O_3 and SiO_2, new electrochemical systems are clearly visible at a higher potential than the Al_2O_3 reduction peak. This significant cathodic current density increase can be attributed to the formation of Si/Al alloys by Under Potential Deposition (UPD) (Brenner, 1963; Kokkinidis, 1986; Taxil et al., 2003; Gibilaro et al., 2008, 2009; Massot et al., 2022), which occurs from a co-reduction between two elements or from reactive electrodeposition. Thus, the only way to deposit Si is through alloy formation.

3.2.2. Under potential deposition evidence for LiF–NaF–Al_2O_3–Fe_2O_3 and LiF–NaF– SiO_2–Al_2O_3–Fe_2O_3

A cyclic voltammogram plotted at 100 mV s^{-1} of 2 wt% Al_2O_3 + 2.6 wt% Fe_2O_3 and 2 wt% Al_2O_3 + 2.6 wt% Fe_2O_3 + 1 wt% SiO_2 can be seen in Fig. 7.

An electrochemical signal is observed for 2 wt% Al_2O_3 + 2.6 wt%

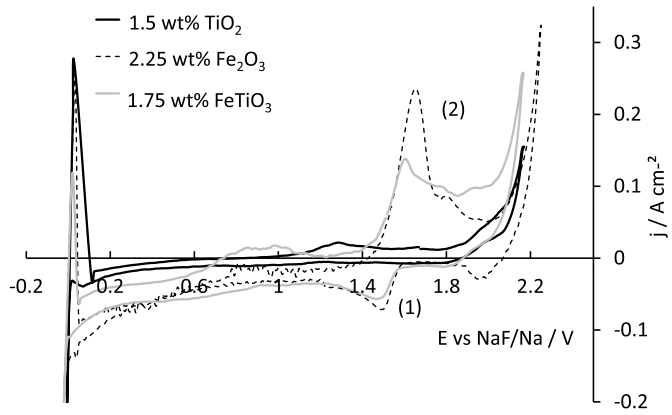

Fig. 5. Cyclic voltammogram of LiF–NaF–TiO_2 (1.5 wt%), LiF–NaF–Fe_2O_3 (2.25 wt%) and LiF–NaF–$FeTiO_3$ (1.75 wt%) systems on Mo electrode at 100 mV s^{-1} and T = 800 °C. The reduction peak at 1.5 V vs NaF/Na is indicated by (1) and the oxidation peak at 1.62 V vs NaF/Na is indicated by (2).

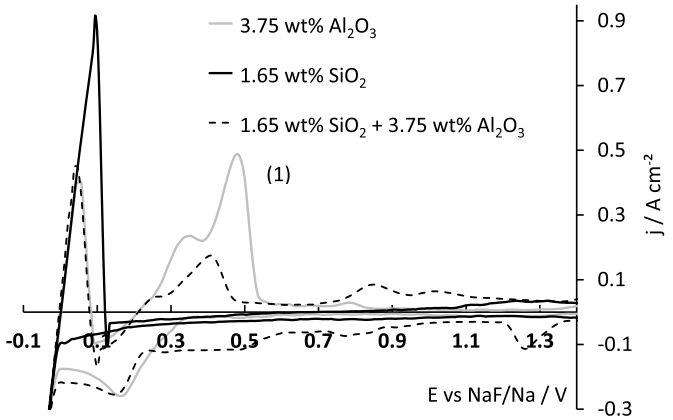

Fig. 6. Cyclic voltammograms of LiF–NaF–Al_2O_3 (3.75 wt%), LiF–NaF–SiO_2 (1.65 wt%) and LiF–NaF–Al_2O_3–SiO_2 (3.75 wt% −1.65 wt%) systems on Mo electrode at 100 mV s^{-1} and T = 800 °C. The oxidation peak at 0.49 V vs NaF/Na is indicated by (1).

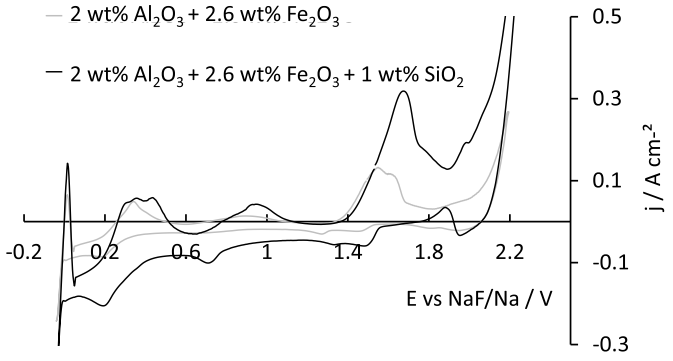

Fig. 7. Cyclic voltammograms of LiF–NaF–SiO_2–Al_2O_3–Fe_2O_3 (1 wt% - 2 wt% - 2.6 wt%) and LiF–NaF–Al_2O_3–Fe_2O_3 (2 wt% - 2.6 wt%) systems on Mo electrode at 100 mV s^{-1} and T = 800 °C.

Fe_2O_3 and the same reactions are observed when the oxides were analysed individually: the Fe(II) system at 1.5 V and the reduction of Al_2O_3 at 0.16 V vs NaF/Na. However, when SiO_2 was added to the mixture containing Fe_2O_3 and Al_2O_3, the current density peaks increased, and new oxidation and reduction peaks were observable at 0.94 and 0.71 V vs NaF/Na, respectively. The reduction peaks can be attributed to the LiF–NaF–SiO_2–Al_2O_3 system already observed in Fig. 6. Moreover, the overall current density of the reactions is more intense because of the formations of alloys between Si, Al and Fe.

To conclude this part, the cyclic voltammograms show that the major oxides SiO_2, MgO, Al_2O_3, and Fe_2O_3 of the lunar soil dissolve in the fluoride melt and were electrochemically observed. Even though SiO_2 is not electroactive, it can be observed in the presence of other oxides due to an alloy formation. However, TiO_2 does not present electrochemical activity in LiF–NaF and also in the presence of iron. The overall conclusion is that metal deposition from these oxides is possible when dissolved in LiF–NaF at 800 °C.

3.2.3. *Electrochemical analysis of natural lunar simulant BPY-N in LiF–NaF at 800 °C*

The electroactivity of the lunar simulant BPY-N in the fluoride salt was verified by cyclic voltammetry on a Mo electrode. A voltammogram at 100 mV s^{-1} of 1.34 wt% lunar simulant in LiF–NaF at 800 °C is shown in Fig. 8.

A complex electrochemical signal is obtained confirming the dissolution of the lunar simulant BPY-N in LiF–NaF at 800 °C. The different

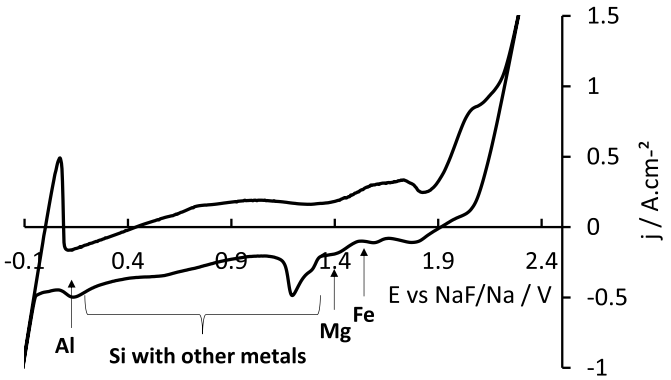

Fig. 8. Cyclic voltammetry of LiF-NaF-BPY-N (1.34 wt%) on Mo electrode at 100 mV s^{-1} and T = 800 °C.

reduction reactions occurring were compared with the previous cyclic voltammograms of the individual oxides and mixtures of those individual oxides in LiF–NaF at 800 °C (See section 3.3.1). The reduction potentials of the individual oxides are indicated in Fig. 8 and correspond to an overview of the BPY-N electrochemical signal.

- Reduction of Fe_2O_3 from 1.5 V vs NaF/Na.
- Reduction of MgO from 1.3 V vs NaF/Na.
- Reduction of Al_2O_3 from 0.3 V vs NaF/Na.
- In between 0.13 and 1.3 V vs NaF/Na, the cathodic current is attributed to Si based alloys formation.

These key observations show that metals can be produced by electrolysis from a lunar mare simulant in the fluoride-based media at 800 °C. Electrodepositions were performed on different substrates to observe and characterize the composition of the metal produced.

3.3. *Deposition of metals with natural lunar simulant BPY-N*

Electrolyses were carried out on Mo, Fe and C in LiF-NaF-BPY-N (4 wt%) at 800 °C. The cathodic products obtained were observed and characterized through SEM-EDX analysis.

3.3.1. *Deposition of dissolved natural lunar simulant BPY-N on Mo and Fe*

Galvanostatic electrolysis at −0.21 A was performed for 3.5 h on molybdenum electrode with a surface area of 0.38 cm^2 (A) and potentiostatic electrolysis at 0.18 V vs NaF/Na was performed for 3.5 h on iron with a surface area of 0.32 cm^2 (B), as presented in Fig. 9. SEM-EDX analyses of the electrodes after electrolysis are shown in Fig. 10.

The potential of the Mo electrode during galvanostatic electrolysis is stable around 0.1 V vs NaF/Na for 3h and then it increases to 0.3 V vs NaF/Na (Fig. 9-A). An adherent layer of metallic compounds made of Si–Mo (65–35 at%) is observed with an average thickness of 23 μm (Fig. 10-A). The unique presence of Si is explained by its high concentration in BPY-N. In fact, SiO_2 represents 42.8 wt% of the BPY-N sample, where Si represents 21.5 mol% of BPY-N.

The electrolysis current density on the Fe electrode is stable for less than an hour at −0.1 A cm^{-2}. After 1h, the current density slowly increases to 0.2 A cm^{-2} (Fig. 9-B). Metallic compounds of Fe–Si (75–25 at %) are obtained but compared to the Mo electrode, no dense layer of metal compounds is evidenced. Instead, sequences of small layers (~ 10 μm) of salt are observed (Fig. 10-B). This phenomenon could be explained by the difference in molar volume, wherein silicon is much more dense than iron (Lu et al., 2005) causing the deposit breakdown.

Thus, these results demonstrate that Si can be efficiently deposited in an alloyed form with Mo and Fe.

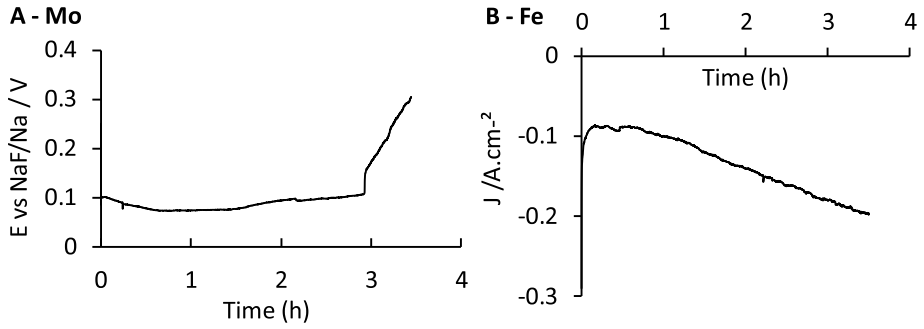

Fig. 9. Galvanostatic electrolysis at −0.21 A on Mo electrode (A) and potentiostatic electrolysis at 0.18 V vs NaF/Na on Fe electrode (B) for 3.5 h in a molten bath of 4% wt BPY-N in LiF–NaF at 800 °C.

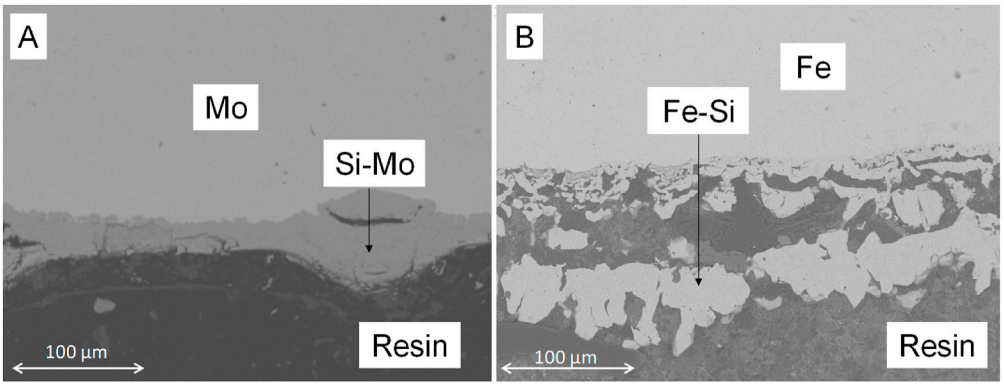

Fig. 10. Cross section SEM analysis of deposits obtained after electrolysis of dissolved lunar simulant BPY-N on Mo electrode (A) and Fe electrode (B).

3.3.2. Carbon electrode

Potentiostatic electrolysis at 0.4 V vs NaF/Na for 3.5 h was performed on carbon with a surface area of 0.94 cm^2. The electrolysis is presented in Fig. 11 and the SEM-EDX analysis is shown in Fig. 12.

During the potentiostatic electrolysis, the current density remained constant at around −0.08 A cm^{-2} for the first 20 min of the electrolysis, from which a steady decrease was observed reaching −0.13 A cm^{-2} (Fig. 11). Carbide compounds made of C–Si–Ti (60-17-23 at%) were formed: titanium was only observed on the C electrode. This key observation implies the feasibility of titanium deposition through UPD on C electrode only.

Furthermore, blocks of Al–Si–Na (33-33-34 at%) were spotted around the electrode, suggesting preferential deposition spots on the electrode (Fig. 12).

For all the electrolyses, a silicon deposit was obtained although pure Si deposition is not observed in LiF–NaF. However, in the presence of other metals, silicon can be deposited in an alloyed form due to UPD. Furthermore, the nature of the electrode changes the materials obtained after deposition. For instance, although silicon is the main product, aluminium and titanium carbides could be obtained if a carbon electrode is used. The possibility of extracting Si through molten salt electrolysis plays a significant role in the future development of this process. Si is abundant in lunar regolith and could be used for the production of solar cells (Duke et al., 2001; Ignatiev and Freundlich, 2012), glass and semiconductors (Landis, 2007) for instance.

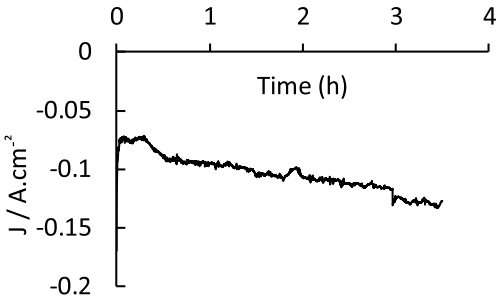

Fig. 11. Potentiostatic electrolysis on carbon electrode in a molten bath of 4% wt BPY-N in LiF–NaF at 800 °C.

3.4. Comparison of BPY-Synthetic-Oxide-Powder (BPY–SOP) with BPY natural (BPY–N)

The use of BPY-SOP intends to assess the potential differences arising in the electrolysis process depending on the crystallinity and microstructural properties of the starting material. The chemical composition of BPY-SOP is indeed similar to the lunar simulant BPY-N and is shown in section 2.5. A cyclic voltammogram of 4 wt% BPY-SOP is compared with 4 wt% lunar simulant BPY-N on Mo electrode at 100 mV s^{-1} in LiF–NaF at 800 °C is shown in Fig. 13.

The electrochemical signals obtained from the produced BPY-SOP are similar to the lunar simulant BPY-N. This can be explained by the fact that the metallic oxides dissolve in the molten bath of LiF–NaF and no crystalline structure remains in the liquid phase. We compared the nature of the metallic deposition for BPY-SOP with BPY-N to confirm their similar behaviour. A galvanostatic electrolysis at 0.06 A for 3.5 h was applied to Mo electrode with a surface area of 0.33 cm^2. The electrolysis and SEM-EDX analyses are shown in Figs. 14 and 15, respectively.

The electrolysis potential is unstable for the first 1.5 h. It increases from the initial 0.22–1.2 V vs NaF/Na and then remains constant (Fig. 14). As seen in Fig. 10, a similar deposition of Si–Mo (62–38 at%) is observed (Fig. 15). The thickness of the layer obtained is around 7 µm.

The same electrochemical signal and deposition are observed

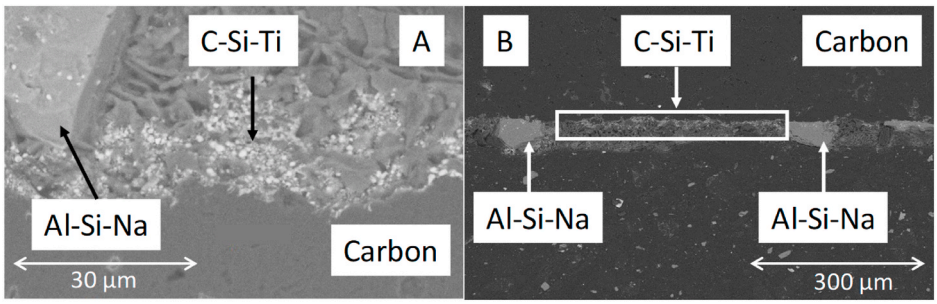

Fig. 12. Cross section SEM analysis of deposits obtained after electrolysis of dissolved lunar simulant on C electrode with two different magnification. The magnification is 10 times more important in image A compared to image B.

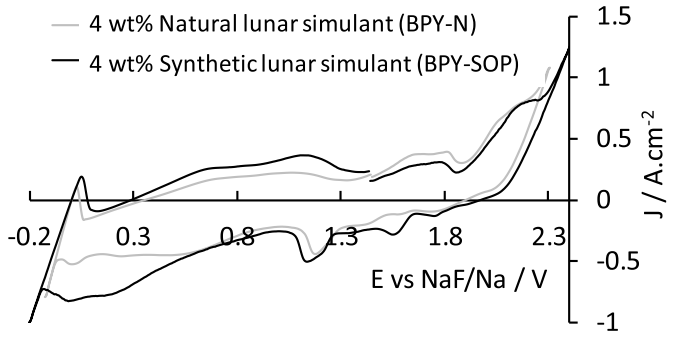

Fig. 13. Comparison of cyclic voltammograms on Mo electrode at 100 mV s^{-1} of natural lunar simulant BPY-N (4 wt%) vs synthetic lunar simulant BPY-SOP (4 wt%) made of mixed powder of the main metallic oxides composing BPY-N in LiF–NaF at 800 °C.

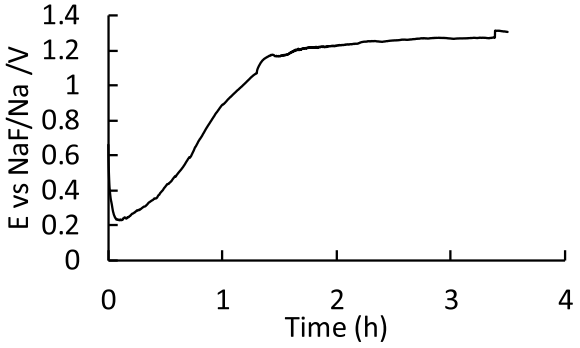

Fig. 14. Galvanostatic electrolysis at 0.06 A on Mo electrode in a molten bath of 4 wt% BPY-SOP in LiF–NaF at 800 °C.

between a crystalline (BPY–N) and a synthetic lunar simulant (BPY–SOP) on Mo electrode. These results provide evidence that a mixture of oxides powders has the same electrochemical behaviour as a crystalline lunar simulant. This shows that the crystalline nature of the lunar soil has no impact on its electrochemical behaviour in LiF–NaF. In essence, the fluoride solvent appears thus not to be critically influenced by the physical state of lunar mare soils (degree of crystallinity) indicating it could be implemented in the lunar environment, without further preparatory steps.

4. Conclusions

A new fluoride-based mixture for molten salt electrolysis was studied for ISRU purposes. Solubility research was performed on a natural lunar simulant BPY-N in LiF–NaF at 800 °C. First, the individual oxides

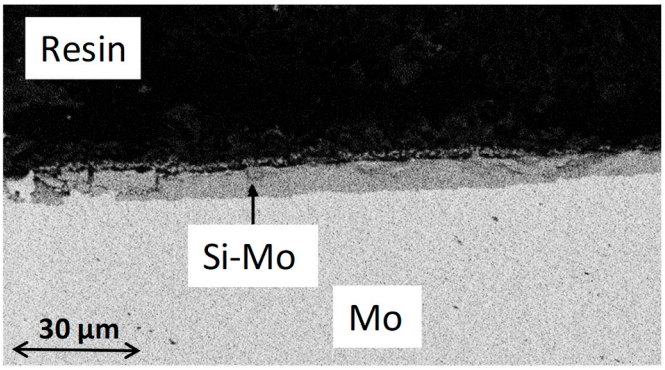

Fig. 15. Cross section SEM analysis of deposits obtained after electrolysis of dissolved BPY-SOP on Mo electrode.

composing the lunar soil (SiO_2, Al_2O_3, Fe_2O_3, MgO, and TiO_2) were studied separately and ICP-AES measurements showed that all the oxides are soluble in the fluoride media with SiO_2 exhibiting the highest solubility (17.4 wt%). When BPY-N was analysed, a joint solubility effect was observed causing a significant decrease in the individual solubility of all the oxides in the LiF–NaF system. A maximum joint solubility was observed for 3.9 wt% LiF-NaF-BPY-N. However, all the BPY-N oxides remained partially soluble in LiF–NaF, meaning it can be used as a solvent for molten salt electrolysis for ISRU research. A working temperature of 800 °C was chosen as a first demonstration but the use of lower working temperatures and their impact on the solubility of the lunar simulant could be investigated.

Furthermore, cyclic voltammograms have shown the electroactivity of all the individual oxides, except of TiO_2 and SiO2 in LiF–NaF. While SiO_2 and TiO_2 are individually not electroactive, they form alloys in the presence of other oxides through under potential deposition phenomenon. The electrochemical system of natural BPY-N was characterized experimentally and compared with the individual oxides, allowing to identify some of the reactions in the BPY-N complex signal. From this lunar simulant, metallic deposits of Si–Mo and Si–Fe were obtained on Mo and Fe electrodes, respectively. Several compounds such as titanium carbides and Si–Al alloys were obtained on C electrode, suggesting that different deposits can be obtained depending on the nature of the cathodic substrate. Synthetic lunar simulant BPY-SOP made of a mixture of the different oxides composing lunar mare soil has the same electrochemical behaviour as a crystalline lunar mare simulant, meaning that raw material can be directly used in this process. Accordingly, any lunar mare soil can be reproduced by simply mixing, with the appropriate chemical composition, the oxides specific to the given location on the Moon: thus, the mixture can be used as a lunar simulant in molten salt technology. Furthermore, the synthetic lunar soil can be doped with specific oxides such as titanium to observe its influence on the process. As a complement, a highland lunar simulant should be studied in the

same way to ascertain this result. Hence, the physical state of the lunar regolith has no critical impact on its dissolution in the fluoride solvent, confirming its adaptability for use on the lunar surface without the necessity of additional steps.

CRediT authorship contribution statement

M. Maes: Investigation, Writing – original draft. **M. Gibilaro:** Investigation, Supervision, Writing – review & editing. **P. Chamelot:** Project administration. **C. Chiron:** Formal analysis. **S. Chevrel:** Writing – review & editing. **P. Pinet:** Writing – review & editing. **L. Massot:** Writing – review & editing. **J.J. Favier:** Methodology.

Declaration of competing interest

The authors declare that they have no known competing financial interests or personal relationships that could have appeared to influence the work reported in this paper.

Data availability

Data will be made available on request.

Acknowledgments

This project was one of the research priorities of the Regolith Toulouse Task Force which comprises the Institut Clément Ader (UMR CNRS 5312), the Institute of Research in Astrophysics and Planetology (IRAP/UMR CNRS 5277) and the Laboratoire Génie Chimique (LGC). The authors express their thanks to Thierry Cutard, Julien Granier, Thierry Sentenac and Yannick le Maoult from ICA for the characterisation of BPY-N. In Memoriam of Jean-Jacques Favier (International Space University, CNES, France) for his involvement and guidance during the project.

References

Allen, C.C., Morris, R.V., McKay, D.S., 1996. Oxygen extraction from lunar soils and pyroclastic glass. J. Geophys. Res. Planets 101, 26085–26095. https://doi.org/10.1029/96JE02726.

Anand, M., Crawford, I.A., Balat-Pichelin, M., Abanades, S., Westrenen, W. van, Péraudeau, G., Jaumann, R., Seboldt, W., 2012. A brief review of chemical and mineralogical resources on the Moon and likely initial in situ resource utilization (ISRU) applications. Planet. Space Sci 74, 42–48. https://doi.org/10.1016/j.pss.2012.08.012.

Bessada, C., Zanghi, D., Salanne, M., Gil-Martin, A., Gibilaro, M., Chamelot, P., Massot, L., Nezu, A., Matsuura, H., 2020. Investigation of ionic local structure in molten salt fast reactor LiF-ThF4-UF4 fuel by EXAFS experiments and molecular dynamics simulations. J. Mol. Liq. 307, 112927 https://doi.org/10.1016/j.molliq.2020.112927.

Electrodeposition of alloys: PRINCIPLES and PRACTICE. In: Brenner, A. (Ed.), 1963. Electrodeposition of Alloys. Academic Press, p. ii. https://doi.org/10.1016/B978-1-4831-9807-1.50001-5.

Cardiff, E.H., Pomeroy, B.R., Banks, I.S., Benz, A., 2007. Vacuum pyrolysis and related ISRU techniques. In: AIP Conf. Proc., vol. 880, pp. 846–853. https://doi.org/10.1063/1.2437525.

Che, X., Nemchin, A., Liu, D., Long, T., Wang, C., Norman, M.D., Joy, K.H., Tartese, R., Head, J., Jolliff, B., Snape, J.F., Neal, C.R., Whitehouse, M.J., Crow, C., Benedix, G., Jourdan, F., Yang, Z., Yang, C., Liu, J., Xie, S., Bao, Z., Fan, R., Li, D., Li, Z., Webb, S. G., 2021. Age and composition of young basalts on the Moon, measured from samples returned by Chang'e-5. Science 374, 887–890. https://doi.org/10.1126/science.abl7957.

Chen, G.Z., Fray, D.J., Farthing, T.W., 2000. Direct electrochemical reduction of titanium dioxide to titanium in molten calcium chloride. Nature 407, 361–364. https://doi.org/10.1038/35030069.

Chen, Y., Hu, S., Li, J.-H., Li, Q.-L., Li, X., Li, Y., Liu, Y., Qian, Y., Yang, W., Zhou, Q., Lin, Y., Li, C., Li, X.-H., 2023. Chang'e-5 lunar samples shed new light on the Moon. Innov. Geosci. 1, 100014–100015. https://doi.org/10.59717/j.xinn-geo.2023.100014.

Cutler, A.H., Krag, P., 1985. A carbothermal scheme for lunar oxygen production. In: Lunar Bases and Space Activities of the 21st Century. Lunar and Planetary Institute, Houston, Texas, p. 559.

Denk, T., González-Pardo, A., Cañadas, I., Vidal, A., 2017. Design and test of a concentrated solar powered fluidized bed reactor for ilmenite reduction. Sol. Power Chem. Energy Syst. 2017.

Duke, M., Ignatiev, A., Freundlich, A., Rosenberg, S., Makel, D., 2001. Silicon PV cell production on the Moon as the basis for new architecture for space exploration. In: AIP Conf. Proc., vol. 552, pp. 19–24. https://doi.org/10.1063/1.1357899.

Ellery, A., Mellor, I., Wanjara, P., Conti, M., 2022. Metalysis Fray farthing chen process as a strategic lunar in situ resource utilization technology. New Space 10, 224–238. https://doi.org/10.1089/space.2021.0047.

Exolith Lab, 2023. Lunar Mare (LMS-1) High-Fidelity Moon Dirt Simulant [WWW Document]. Exolith Lab. URL. https://exolithsimulants.com/products/lms-1-lunar-mare-simulant, 1.24.23.

Feng, Y., Li, M., Hou, W., Cheng, B., Wang, J., Li, H., 2021. First-principles molecular dynamics simulation on high silica content Na3AlF6–Al2O3–SiO2 molten salt. ACS Omega 6, 3745–3751. https://doi.org/10.1021/acsomega.0c05339.

Fray, D.J., 1999. Removal of Oxygen from Metal Oxides and Solid Solutions by Electrolysis in a Fused Salt. Int. Pat. WO 9964638.

Gibilaro, M., Massot, L., Chamelot, P., Taxil, P., 2009. Electrochemical preparation of aluminium–nickel alloys by under-potential deposition in molten fluorides. J. Alloys Compd. 471, 412–420. https://doi.org/10.1016/j.jallcom.2008.03.115.

Gibilaro, M., Massot, L., Chamelot, P., Taxil, P., 2008. Study of neodymium extraction in molten fluorides by electrochemical co-reduction with aluminium. J. Nucl. Mater. 382, 39–45. https://doi.org/10.1016/j.jnucmat.2008.09.004.

Gibson, M., Knudsen, C.W., Brueneman, D.J., Allen, C., Kanamori, H., Mckay, D., 1994. Reduction of lunar basalt 70035: oxygen yield and reaction product analysis. J. Geophys. Res. 99, 10887–10897.

Gmitter, A.J., 2008. The Influence of Inert Anode Material and Electrolyte Composition on the Electrochemical Production of Oxygen from Molten Oxides (PhD Thesis). Massachusetts Institute of Technology.

Gordon, P., Colozza, A., Hepp, A., Heller, R., Gustafson, R., Stern, T., Nakamura, T., 2011. Thermal energy process heat for lunar ISRU: technical challenges and technology opportunities. In: 49th AIAA Aerospace Sciences Meeting Including the New Horizons Forum and Aerospace Exposition, p. 704.

Granier, J., Cutard, T., Pinet, P., Le Maoult, Y., Sentenac, T., Chevrel, S.D., 2022. Characterization and physical properties of a lunar regolith analog for powder bed fusion-based additive manufacturing processes. In: European Lunar Symposium 10th, European Lunar Symposium 10th Abstract Booklet. En ligne, France, pp. 127–128.

Gu, L., Lin, Y., Chen, Y., Xu, Y., Tang, X., Hu, S., Mao, H., Li, J., 2023. Measurement of ferric iron in Chang'e-5 impact glass beads. Earth Planets Space 75, 151. https://doi.org/10.1186/s40623-023-01909-1.

Hegde, U., Balasubramaniam, R., Gokoglu, S., 2009. Development and validation of a model for hydrogen reduction of JSC-1A. In: 47th AIAA Aerospace Sciences Meeting Including the New Horizons Forum and Aerospace Exposition, Aerospace Sciences Meetings. American Institute of Aeronautics and Astronautics. https://doi.org/10.2514/6.2009-1389.

Ignatiev, A., Freundlich, A., 2012. The use of lunar resources for energy generation on the moon. In: Moon: Prospective Energy and Material Resources, pp. 325–334. https://doi.org/10.1007/978-3-642-27969-0_13.

Isachenkov, M., Chugunov, S., Landsman, Z., Akhatov, I., Metke, A., Tikhonov, A., Shishkovsky, I., 2022a. Characterization of novel lunar highland and mare simulants for ISRU research applications. Icarus 376, 114873. https://doi.org/10.1016/j.icarus.2021.114873.

Isachenkov, M., Chugunov, S., Smirnov, A., Kholodkova, A., Akhatov, I., Shishkovsky, I., 2022b. The effect of particle size of highland and mare lunar regolith simulants on their printability in vat polymerisation additive manufacturing. Ceram. Int. 48, 34713–34719. https://doi.org/10.1016/j.ceramint.2022.08.060.

Kate, I.L. ten, Cardiff, E.H., Dworkin, J.P., Feng, S.H., Holmes, V., Malespin, C., Stern, J. G., Swindle, T.D., Glavin, D.P., 2010. VAPoR – volatile Analysis by Pyrolysis of Regolith – an instrument for in situ detection of water, noble gases, and organics on the Moon. Planet. Space Sci. 58, 1007–1017. https://doi.org/10.1016/j.pss.2010.03.006.

Kesterke, D.G., 1971. Electrowinning of Oxygen from Silicate Rocks. U.S. Department of Interior, Bureau of Mines.

Kim, H., Paramore, J., Allanore, A., Sadoway, D.R., 2011. Electrolysis of molten iron oxide with an iridium anode: the role of electrolyte basicity. J. Electrochem. Soc. 158, E101. https://doi.org/10.1149/1.3623446.

Kobayashi, Y., Sonezaki, H., Endo, R., Susa, M., 2010. Reduction kinetics of iron oxides in molten lunar soil simulant by graphite. ISIJ Int. 50, 35–43. https://doi.org/10.2355/isijinternational.50.35.

Kokkinidis, G., 1986. Underpotential deposition and electrocatalysis. J. Electroanal. Chem. Interfacial Electrochem. 201, 217–236. https://doi.org/10.1016/0022-0728(86)80051-1.

Kumai, E., Tanaka, M., Watanabe, T., Hoshino, T., Hosoda, S., Kanamori, H., 2021. A continuous hydrogen reduction process for the production of water on the Moon. Int. J. Microgravity Sci. Appl. 38, 380203.

Kuznetsova, S.V., Dolmatov, V.S., Kuznetsov, S.A., 2009. Voltammetric study of electroreduction of silicon complexes in a chloride-fluoride melt. Russ. J. Electrochem. 45, 742–748. https://doi.org/10.1134/S1023193509070052.

Landis, G.A., 2007. Materials refining on the moon. Acta Astronaut. 60, 906–915. https://doi.org/10.1016/j.actaastro.2006.11.004.

Li, C., Hu, H., Yang, M.-F., Pei, Z.-Y., Zhou, Q., Ren, X., Liu, B., Liu, D., Zeng, X., Zhang, G., Zhang, H., Liu, J., Wang, Q., Deng, X., Xiao, C., Yao, Y., Xue, D., Zuo, W., Su, Y., Wen, W., Ouyang, Z., 2022. Characteristics of the lunar samples returned by the Chang'E-5 mission. Natl. Sci. Rev. 9, nwab188. https://doi.org/10.1093/nsr/nwab188.

Lim, S., Degli-Alessandrini, G., Bowen, J., Anand, M., Cowley, A., 2023. The microstructure and mechanical properties of microwave-heated lunar simulants at

different input powers under vacuum. Sci. Rep. 13, 1804. https://doi.org/10.1038/s41598-023-29030-z.
Ling, Z., Jolliff, B.L., Wang, A., Li, C., Liu, Jianzhong, Zhang, J., Li, B., Sun, L., Chen, J., Xiao, L., Liu, Jianjun, Ren, X., Peng, W., Wang, H., Cui, X., He, Z., Wang, J., 2015. Correlated compositional and mineralogical investigations at the Chang'e-3 landing site. Nat. Commun. 6, 8880. https://doi.org/10.1038/ncomms9880.
Liu, A., Shi, Z., Hu, X., Gao, B., Wang, Z., 2017. Lunar soil simulant electrolysis using inert anode for Al-Si alloy and oxygen production. J. Electrochem. Soc. 164, H126–H133. https://doi.org/10.1149/2.1381702jes.
Lizin, A.A., Tomilin, S.V., Naumov, V.S., Ignat'ev, V.V., Nezgovorov, N.Yu, Baranov, A. Yu, 2015. Joint solubility of PuF3 and UF4 in a melt of lithium, sodium, and potassium fluorides. Radiochemistry 57, 498–503. https://doi.org/10.1134/S1066362215050082.
Lomax, B.A., Conti, M., Khan, N., Bennett, N.S., Ganin, A.Y., Symes, M.D., 2020. Proving the viability of an electrochemical process for the simultaneous extraction of oxygen and production of metal alloys from lunar regolith. Planet. Space Sci. 180, 104748 https://doi.org/10.1016/j.pss.2019.104748.
Lu, X.-G., Selleby, M., Sundman, B., 2005. Assessments of molar volume and thermal expansion for selected bcc, fcc and hcp metallic elements. Calphad 29, 68–89. https://doi.org/10.1016/j.calphad.2005.05.001.
Lu, Y., Mantha, D., Reddy, R.G., 2010. Thermodynamic analysis on lunar soil reduced by hydrogen. Metall. Mater. Trans. B 41, 1321–1327. https://doi.org/10.1007/s11663-010-9411-3.
Lu, Y., Reddy, R.G., 2008. Extraction of metals and oxygen from lunar soil. High Temp. Mater. Process. 27, 223–234.
Massot, L., Meskine, H., Gibilaro, M., Chamelot, P., 2022. Electrochemical co-deposition of Erbium and Ytterbium in molten LiF-CaF2: an original way for lanthanides extraction on inert electrode. J. Fluor. Chem. 257–258, 109977 https://doi.org/10.1016/j.jfluchem.2022.109977.
McKay, D.S., Heiken, G., Basu, A., Blanford, G., Simon, S., Reedy, R., French, B.M., Papike, J., 1991. The lunar regolith. In: Lunar Sourcebook. Cambridge University Press, New-York, pp. 285–356.
Meurisse, A., Lomax, B., Selmeci, Á., Conti, M., Lindner, R., Makaya, A., Symes, M.D., Carpenter, J., 2022. Lower temperature electrochemical reduction of lunar regolith simulants in molten salts. Planet. Space Sci. 211, 105408 https://doi.org/10.1016/j.pss.2021.105408.
Mysen, B.O., Virgo, D., 1985. Interaction between fluorine and silica in quenched melts on the joins SiO2-AlF3 and SiO2-NaF determined by Raman spectroscopy. Phys. Chem. Miner. 12, 77–85. https://doi.org/10.1007/BF01046830.
Palos, M.F., Serra, P., Fereres, S., Stephenson, K., González-Cinca, R., 2020. Lunar ISRU energy storage and electricity generation. Acta Astronaut. 170, 412–420. https://doi.org/10.1016/j.actaastro.2020.02.005.
Papike, J.J., Simon, S.B., Laul, J.C., 1982. The lunar regolith: chemistry, mineralogy, and petrology. Rev. Geophys. 20, 761–826. https://doi.org/10.1029/RG020i004p00761.
Peng, Y., Tang, H., Mo, B., Zeng, X., Miao, B., 2022. Influencing factors for the preparation of Fe0 in lunar soil simulant using high-temperature carbothermic reduction. Adv. Space Res. 70, 3220–3230. https://doi.org/10.1016/j.asr.2022.07.074.
Rosenberg, S.D., Beegle Jr., R.L., Guter, G.A., Miller, F.E., Rothenberg, M., 1992. The onsite manufacture of propellant oxygen from lunar resources. NASA Johns. Space Cent. Space Resour. 3, 162–185.
Sanders Gerald, B., Larson William, E., 2013. Progress made in lunar in situ resource utilization under NASA's exploration technology and development program. J. Aero. Eng. 26, 5–17. https://doi.org/10.1061/(ASCE)AS.1943-5525.0000208.
Sargeant, H.M., Barber, S.J., Anand, M., Abernethy, F.A.J., Sheridan, S., Wright, I.P., Morse, A.D., 2021. Hydrogen reduction of lunar samples in a static system for a water production demonstration on the Moon. Planet. Space Sci. 205, 105287 https://doi.org/10.1016/j.pss.2021.105287.
Sargeant, H.M., Schultz, J., Moser-Mancewicz, N., Long-Fox, J., Ustunisik, G.K., Nielsen, R.L., Britt, D., 2022. Lunar simulant considerations for molten regolith electrolysis experiments. In: 53rd Lunar and Planetary Science Conference. LPI Contributions, p. 2048.
Schein, V., Witchalls, J., Lomax, B., Mcdonald, F., Starr, S., Hadler, K., Cilliers, J., 2022. Vibration-induced segregation ("Brazil-Nut" effect) of the lunar regolith to control particle size for In-Situ Resource Utilization applications. In: 44th COSPAR Scientific Assembly, p. 141. Held 16-24 July.
Schlüter, L., Cowley, A., 2020. Review of techniques for In-Situ oxygen extraction on the moon. Planet. Space Sci. 181, 104753 https://doi.org/10.1016/j.pss.2019.104753.
Schubert, P.J., 2007. Oxygen Separation from Lunar Regolith (SAE Technical Paper No. 2007- 01–3107). SAE International, Warrendale, PA. https://doi.org/10.4271/2007-01-3107.
Schwandt, C., Doughty, G.R., Fray, D.J., 2010. The FFC-Cambridge process for titanium metal winning. Key Eng. Mater. 436, 13–25. https://doi.org/10.4028/www.scientific.net/KEM.436.13.
Schwandt, C., Hamilton, J.A., Fray, D.J., Crawford, I.A., 2012. The production of oxygen and metal from lunar regolith. Planet. Space Sci. 74, 49–56. https://doi.org/10.1016/j.pss.2012.06.011.
Sen, S., Ray, C.S., Reddy, R.G., 2005. Processing of lunar soil simulant for space exploration applications. Mater. Sci. Eng., A 413–414, 592–597. https://doi.org/10.1016/j.msea.2005.08.172.
Senior, C., 1992. Lunar oxygen production by pyrolysis. In: Space Programs and Technologies Conference. AIAA SPACE Forum. American Institute of Aeronautics and Astronautics. https://doi.org/10.2514/6.1992-1663.
Shaw, M., Humbert, M., Brooks, G., Rhamdhani, A., Duffy, A., Pownceby, M., 2022. Mineral processing and metal extraction on the lunar surface - challenges and opportunities. Miner. Process. Extr. Metall. Rev. 43, 865–891. https://doi.org/10.1080/08827508.2021.1969390.
Shaw, M.G., Brooks, G.A., Rhamdhani, M.A., Duffy, A.R., Pownceby, M.I., 2021. Thermodynamic modelling of ultra-high vacuum thermal decomposition for lunar resource processing. Planet. Space Sci. 204, 105272 https://doi.org/10.1016/j.pss.2021.105272.
Shi, H., Li, P., Yang, Z., Zheng, K., Du, K., Guo, L., Yu, R., Wang, P., Yin, H., Wang, D., 2022. Extracting oxygen from chang'e-5 lunar regolith simulants. ACS Sustain. Chem. Eng. 10, 13661–13668. https://doi.org/10.1021/acssuschemeng.2c03545.
Sibille, L., Sadoway, D., Sirk, A., Tripathy, P., Melendez, O., Standish, E., Dominguez, J., Stefanescu, D., Curreri, P., Poizeau, S., 2009. Recent advances in scale-up development of molten regolith electrolysis for oxygen production in support of a lunar base. In: 47th AIAA Aerospace Sciences Meeting Including the New Horizons Forum and Aerospace Exposition, p. 659.
Souchon, A.L., Pinet, P.C., Chevrel, S.D., Daydou, Y.H., Baratoux, D., Kurita, K., Shepard, M.K., Helfenstein, P., 2011. An experimental study of Hapke's modeling of natural granular surface samples. Icarus 215, 313–331. https://doi.org/10.1016/j.icarus.2011.06.023.
Steurer, W., Nerad, B., 1983. Vapor Phase Reduction. Res. Use Space Resour. Ed WF Carroll NASA JPL Publ 83–36.
Taxil, P., Chamelot, P., Massot, L., Hamel, C., 2003. Electrodeposition of alloys or compounds in molten salts and applications. J. Min. Metall. B Metall. 39, 177–200.
Taylor, L.A., Liu, Y., 2010. Important considerations for lunar soil simulants. In: Earth and Space 2010: Engineering, Science, Construction, and Operations in Challenging Environments, pp. 106–118.
Taylor, L.A., Pieters, C.M., Britt, D., 2016. Evaluations of lunar regolith simulants. Planet. Space Sci. 126, 1–7. https://doi.org/10.1016/j.pss.2016.04.005.
Troisi, I., Lunghi, P., Lavagna, M., 2022. Oxygen extraction from lunar dry regolith: thermodynamic numerical characterization of the carbothermal reduction. Acta Astronaut. 199, 113–124. https://doi.org/10.1016/j.actaastro.2022.07.021.
Vai, A., Yurko, J., Wang, D., Sadoway, D., 2010. Molten oxide electrolysis for lunar oxygen generation using in situ resources. Miner. Met. Mater. Soc. 301–308, 420 Commonw. Dr P O Box 430 Warrendale PA 15086 USAnpp. 14–18 Feb.
Williams, R.J., 1985. Oxygen extraction from lunar materials: an experimental test of an ilmenite reduction process. In: Lunar Bases and Space Activities of the 21st Century. Lunar and Planetary Institute, Houston, Texas, p. 551.
Xie, K., Shi, Z., Xu, J., Hu, X., Gao, B., Wang, Z., 2017. Aluminothermic reduction-molten salt electrolysis using inert anode for oxygen and Al-base alloy extraction from lunar soil simulant. JOM - J. Miner. Met. Mater. Soc. 69, 1963–1969. https://doi.org/10.1007/s11837-017-2478-4.
Zhang, P., Dai, W., Niu, R., Zhang, G., Liu, G., Liu, X., Bo, Z., Wang, Z., Zheng, H., Liu, C., Yang, H., Bai, Y., Zhang, Y., Yan, D., Zhou, K., Gao, M., 2023. Overview of the lunar in situ resource utilization techniques for future lunar missions. Space Sci. Amp Technol. 3, 37. https://doi.org/10.34133/space.0037.